Near-field dynamics of broad area diode laser at very high pump levels

Martin Hempel,[1,a] Jens W. Tomm,[1] Martina Baeumler,[2] Helmer Konstanzer,[2] Jayanta Mukherjee,[3] and Thomas Elsaesser[1]
[1]*Max-Born-Institut, Max-Born-Str. 2 A, 12489 Berlin, Germany*
[2]*Fraunhofer Institut für Angewandte Festköperphysik, Tullastrasse 72, 79108 Freiburg, Germany*
[3]*Advanced Technology Institute, University of Surrey, Guildford, GU2 7XH, UK*

Near-field properties of the emission of broad area semiconductor diode lasers under extremely high pumping of up to ∼50 times the threshold are investigated. A transition from a gain to thermally-induced index guiding is shown under operation with single pulses of 300 ns duration. At highest output powers, catastrophic optical damage is observed which is studied in conjunction with the evolution of time-averaged filamentary near-field properties. Dynamics of the process is resolved on a picosecond time scale.

Many diode laser applications such as pumping of solid state lasers[1] or ignition of explosives[2] require high optical powers during a short period. Diode lasers operated in a pulsed mode meet these requirements. They can be driven at elevated power levels, well above the power specified for continuous wave (cw) operation. Operation at high power may, e.g., reduce the number of pump diodes necessary in a system,[3] thus save costs and reduce system size.

The *optical near-field intensity* [henceforth referred to as just the near-field (NF)] of a diode laser is a key parameter since it determines the beam properties of the device. Its behavior at high power levels, in particular its temporal evolution under high-current pulses, is still not well understood. Up to now, dynamics of the NF have been investigated up to ∼23 times the lasing threshold for a ridge waveguide,[4] and up to ∼2 times lasing threshold in broad area (BA) lasers.[5] With the current state-of-the-art devices employing modern facet passivation techniques, higher pump levels are readily achievable. However, under extremely high pumping, a further power increase can result in device failure via catastrophic optical damage (COD) of the laser facet.[6] COD is a sudden degradation mechanism. After reaching a critical temperature T_{crit} of 120-160 °C, see Ref. 6, a small volume at the laser facet becomes highly absorbing for the laser light. This leads to a fast temperature rise at the COD site, the so-called *thermal runaway*, by transferring a part of the energy from the light field to the defect volume.

In this Letter, we present new results on the NF dynamics of BA diode lasers being operated at currents of up to ∼50 times the lasing threshold. We study the NF filamentation and interpret its transient evolution. The COD process is investigated and the COD dynamics are analyzed with picosecond time resolution.

Gain-guided BA high-power AlGaAs/GaAs quantum well diode lasers emitting at 808 nm are investigated. They are mounted *p*-side down and have a 50 μm wide and 1.4 mm long emitter stripe. Their front and rear facets have a standard anti-reflective and high-reflective coating, respectively. The devices have a threshold current of (0.21 ± 0.1) A and are specified for cw operation with an emission power of (0.52 ± 0.01) W at 0.6 A. More details are given in Ref. 7

[a]Author to whom correspondence should be addressed. Electronic mail: hempel@mbi-berlin.de

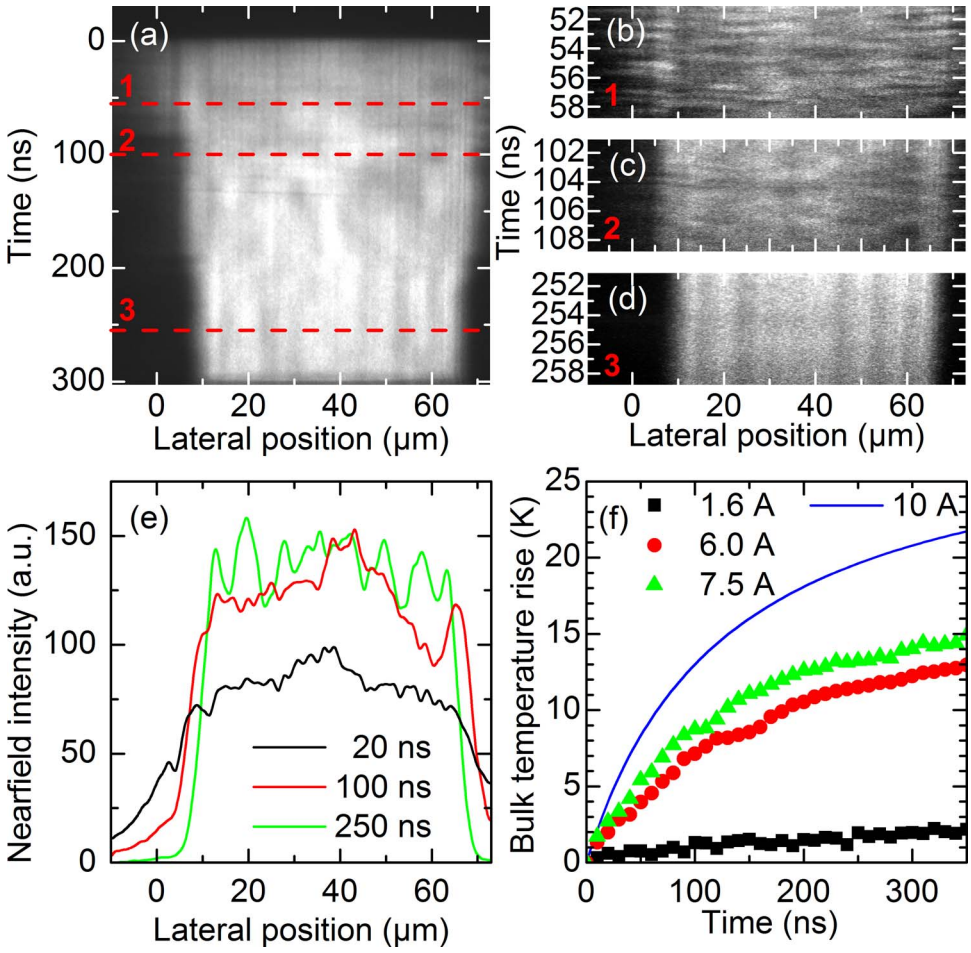

FIG. 1. (a-d) NF images of a device where no damage occurs during the pulse as obtained by the streak-camera. Temporal positions of images (b-d) are indicated in (a) by dashed lines and numbers. (a) Overview along the 300 ns long pulse at 8.5 A. (b) NF evolution at the leading edge of the pulse. (c) NF evolution in the central part of the pulse. (d) NF evolution at the trailing edge of the pulse. (e) Time averaged NF's at different points in time along the 300ns pulse, extracted from (a). (f) Time development of the averaged bulk temperature for different operation currents.

For monitoring the NF, the front facet of the BA laser is imaged onto the input slit of a Hamamatsu streak camera C1587 (with single sweep module M1953) by a microscope objective. This setup allows for a spatial mapping of ∼240 nm per camera pixel. Single pulse step tests are performed. A pulse length of 300 ns is used, while the current for the successive single pulse measurements are increased stepwise by 0.5 A. For testing the device status a single *probe pulse* at a current as low as 1.6 A is applied after each current step. Details of this approach have been described elsewhere.[7,8]

Figures 1(a)–1(d), show the NF dynamics from one of the investigated devices at 8.5 A, i.e., at ∼40 times threshold current. Figure 1(a) covers the entire duration of the current pulse of 300 ns (temporal resolution ∼675 ps). Figures 1(b)–1(d) show details for two different delay times with an increased temporal resolution of ∼18 ps. Obviously, the filamentation characteristics of the NF changes during the pulse. Figure 1(e) shows lateral cuts through the emission plotted in Fig. 1(a). Transients of the bulk temperature of the device are shown in Fig. 1(f) for different operating currents. They were extracted from measurements of the emission wavelength shift. The thermal transient at 10 A is extrapolated from the experimental data taken at lower currents.

Figure 2 shows the time evolution of the NF prior to and during a COD event at 10 A, corresponding to ∼50 times threshold. The upper panels give the NF evolution within (a) the pulse

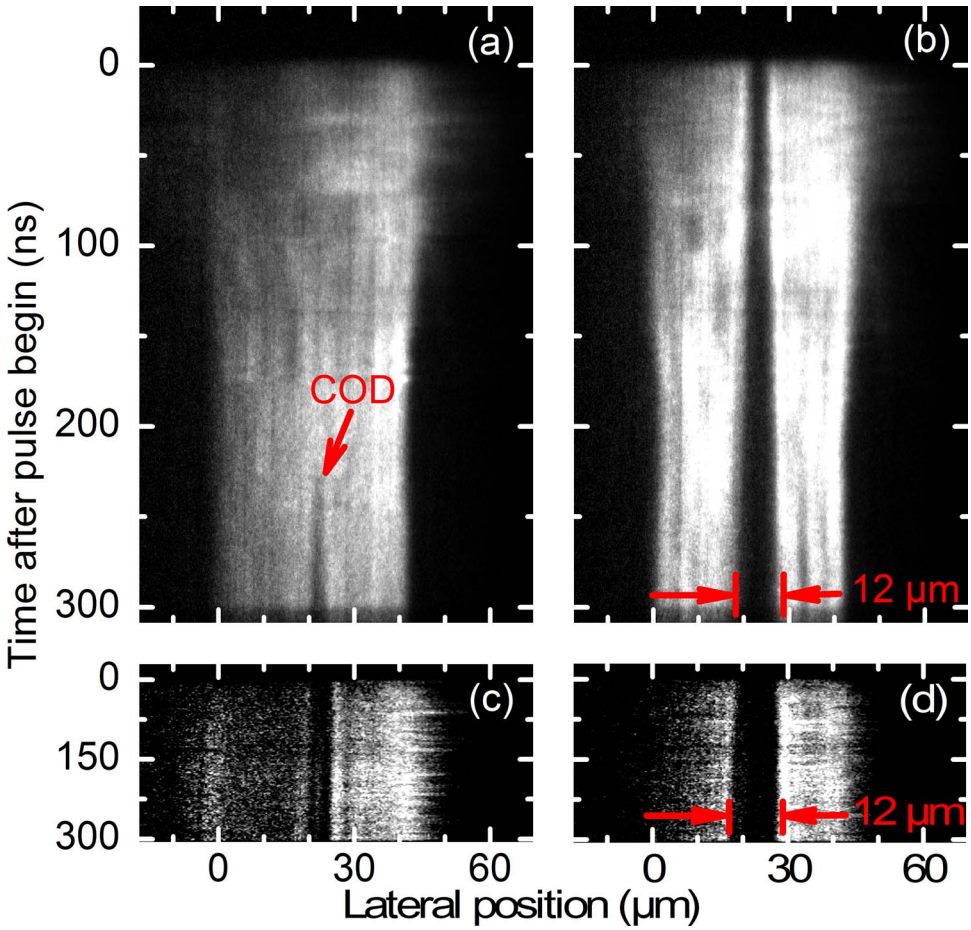

FIG. 2. (a) NF of laser emission during a pulse where COD occurs for first time (10 A). The beginning of COD is marked by an arrow. (b) NF evolution during the following pulse including COD re-ignition. (c) NF evolution during check pulse after the first COD event. (d) NF evolution during check pulse after the following pulse with COD re-ignition.

initiating COD, and (b) the following single pulse which re-ignites the COD process. The lower panels verify the width of the NF gap (area of reduced NF intensity generated by the COD) within the low-power probe pulses.

After such measurements, the device is opened by mechanically removing the n-contact and selective etching of the GaAs substrate and buffer layer.[9] This allows to inspect the QW plane by micro-photoluminescence (μPL); see Fig. 3(a). The expansion of the COD site is seen as dark area with an internal width of 11 μm. From the NF images (Fig. 2), we extract the data given in Figs. 3(b)–3(d). For the COD site, a power decay time of $\tau_{\mathrm{P}} = 33$ ns is extracted, whereas the decay of the integrated output power is represented by $\tau_{\mathrm{P,int}} = 180$ ns (Fig. 3(c)). Panel (c) compares the actual *COD transient* with one where no COD took place. Figure 3(d) quantifies the lateral expansion of the damage site for the two pulses.

We first discuss the transient NF behavior in absence of COD. Figure 1(e) shows that the width of the NF is reduced with increasing temperature of the active region [Fig. 1(f)]. This change occurs at almost constant power, verified by the nearly constant area under the curves in Fig. 1(e), resulting in a higher optical power density at the facet. Additionally, the zig-zag like motion of the main filaments[5,10] becomes imperceptible with increasing temperature [Fig. 1(b)–1(d)]. We attribute this to an increasing frequency of the spatio-temporal lateral field dynamics. After 300 ns, a refractive index rise $\Delta n = 6.5 \times 10^{-3}$ is expected for the active region (at 10 A). This value follows from the extrapolated thermal transient [Fig. 1(f)] and the known dn/dT.[11] These facts indicate a transition

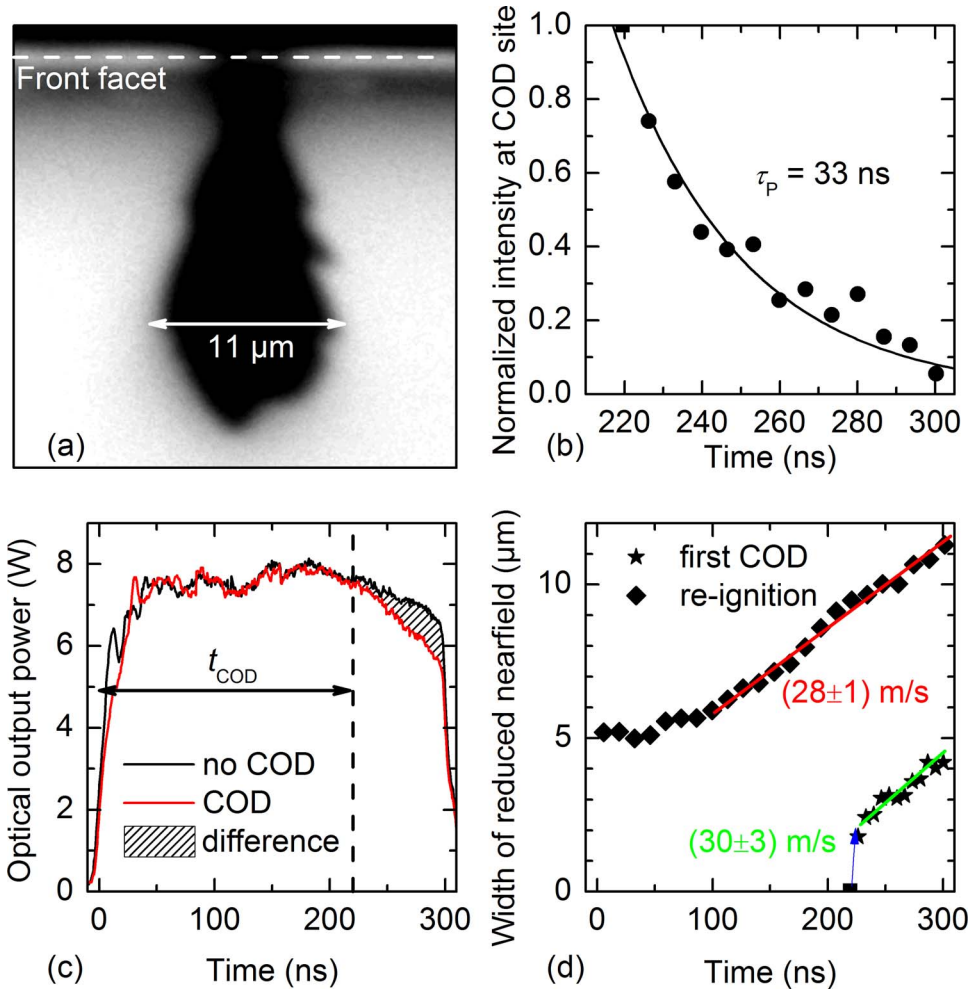

FIG. 3. (a) μPL image of the quantum well emission at the defect site after having experienced the two pulses. The position of the front facet is indicated. (b) Temporal evolution of the normalized intensity at COD site during the initial COD ignition. (c) Integrated optical output power transient during first COD event. (d) Temporal evolution of the NF gap during first COD ignition and subsequent re-ignition. The blue arrow marks the beginning of the process that we refer to as initial thermal runaway.

from pure gain-guiding to thermally-induced index-guiding, as has been suggested by theoretical modeling.[12]

For another device, the COD occurred well within the index-guided regime [10 A, Fig. 2(a)]. The observed $\tau_{P,int}$= 180 ns matches the values obtained during spatially integrated measurements with a fast photodiode for similar devices.[13] The value of $\tau_P = 33$ ns is close to the smallest value ever observed for this type of device in a situation, when almost the entire emitter width was affected by COD.[13] Thus, it is highly likely that the *local decay time* $\tau_P = 33$ ns (at the defect site) is the time the material needs to become (locally) opaque for laser emission. The comparison of the lateral extension of the μPL damage pattern [Fig. 3(a), width 11 μm] with the final width of 12 μm of lowered NF intensity [probe pulse, Fig. 2(d)] gives excellent agreement. We conclude that the transient NF reflects the temporal evolution of the lateral damage site growth, which is closely related to the material parameters.[14]

Considering the evolution of the damage width during the initial COD event [Fig. 3(d)], the damage process begins with a ≤ 2 μm wide defect being created in less than 700 ps. This appears to represent the *kinetics of the thermal runaway.* Subsequent defect growth continues with a constant velocity of (30±3) μm/μs. This indicates that there is no significant reduction in energy driving the

process and no inhomogeneities (induced by the process or grown-in) in the material. The latter view is additionally supported by the symmetric extension of the NF gap to both sides. The probe pulse following the single pulse experiments verifies the damage width. During the following single pulse experiment the damage width remains constant for the first 100 ns [Fig. 3(d)]. This time is needed to provide energy for re-igniting the COD process, as we will show later. Then the damage growth velocity during re-ignition reaches the same value as in the initial COD-pulse. This indicates that the process stops at the end of the COD pulse and now contributes as if unaffected by the trailing edge of the pulse. At the end we have the same resulting damage as in the case of a ~500 ns long pulse (2 pulses each 300 ns minus 100 ns to restore the thermal situation after the initial COD pulse). This justifies the idea to decelerate the COD process[7,8,15] by time-slicing a single current pulse into a sequence of short pulses.

We now consider the energy balance of the COD process. On the sub-microsecond time scale, heat transport within the device plays a minor role and is neglected in the following. The COD starts at t_{COD} after the onset of the pump pulse [Fig. 3(c)]. The integral of the difference between the power $P_{\mathrm{exp}}(t)$ from an intact device and the measured one $P_{\mathrm{meas}}(t)$ [indicated in Fig. 3(c)] from t_{COD} to the end of the pulse (t_{end}) gives the energy W_{mis}, missing in the output:

$$W_{mis} = \int_{t_{COD}}^{t_{end}} [P_{\mathrm{exp}}(t) - P_{meas}(t)]dt. \tag{1}$$

We calculate values of $W_{\mathrm{mis,COD}} = 45$ nJ and $W_{\mathrm{mis,reig}} = 246$ nJ for the COD pulse and the following one, respectively. For comparison, the energy W_{dam} needed for melting the damage site is calculated from

$$W_{dam} = c \cdot \rho \cdot V \cdot \Delta T, \tag{2}$$

with the specific heat $c = 0.33$ J/(gK) and mass density $\rho = 5.33$ g/cm^3. The value for the temperature difference $\Delta T = 1217$ K is taken from Ref. 13 The defect volume V is the damaged area A_{dark} in the emitter plane times a thickness of 1 μm (~ waveguide thickness). The value for the final defective area $A_{\mathrm{dark,final}} = 139\ \mu\mathrm{m}^2$ is taken from the μPL measurement [Fig. 3(a)]. It consists of two parts; $A_{\mathrm{dark,COD}}$ created during the COD-pulse, and $A_{\mathrm{dark,reig}}$ during the pulse where the process re-ignites. Due to the fact that the width of the COD-induced NF gap agrees well with the lateral defect dimension and its linear growth, $A_{\mathrm{dark,COD}}$ can be estimated to 23 μm^2 by scaling $A_{\mathrm{dark,final}}$, while $A_{\mathrm{dark,reig}} = A_{\mathrm{dark,final}}$ - $A_{\mathrm{dark,COD}} = 116\ \mu\mathrm{m}^2$. This leads to energies of $W_{\mathrm{dam,COD}} = 49$ nJ and $W_{\mathrm{dam,reig}} = 248$ nJ required for melting the damaged volume. The latter numbers are in very good agreement with the values W_{mis} derived from the experiment. Thus, the optical output power loss is fully accumulated in defect growth indeed. Note that this picture is valid only as long as the width of the defect is small compared to the emitter width.

We now estimate the energy required to re-ignite the process: Taking 100 ns as heating time for re-ignition [the time interval during which the NF gap does not enlarge; Fig. 2(b)] and a COD-induced output power drop of ~1 W [Fig. 3(c)], we estimate a value of ~100 nJ. Compared to the values estimated above for initial COD ignition (~50 nJ), this value is almost twice as high. Explanations for this difference are:

- In addition to the primary damage detected by μPL [Fig. 3(a)], a cloud of point defects is created around.[7] These defects absorb energy without heating the region around the primary damage to a temperature above T_{crit}. Thus this energy is lost in the energy balance that is made for the primary damage region.
- After an initial defect is created, there is mode re-distribution in the cavity. As a result, we observe an *increased NF intensity* at (still) undamaged facet areas.[7,13] This in turn results in a lower than expected power density at the initial defect.

The latter effect has another important consequence: It can create new COD starting points at the facet after an initial defect is created somewhere at the facet. Since this type of *defect spread* is imparted by the light field, its propagation velocity is extremely fast compared to any other defect growth mechanisms discussed up to now, see Fig. 3(d).

Now it is also possible to calculate the minimal current necessary to re-ignite the process during a 300 ns long pulse and we get 2.8 A. Therefore, the 1.6 A probe pulse is not able to re-ignite COD.

In conclusion, our experiments at extremely high pumping levels show a clear change from a gain to a thermally induced index guided regime. This increases the optical load at the facet and therefore the *facet temperature*. Additionally, a distinct rise in the *bulk temperature* is measured. Together, these two sources enable a microscopic part of the facet ($\leq 2\ \mu$m) to reach T_{crit}. Once the COD process is ignited, the output power drops mainly due to the lateral growth of the damaged site. A characteristic decay time of 180 ns is found in line with values found for similar material systems earlier. The velocity of the lateral motion is determined to 30 μm/μs, while the primary damage of $\leq 2\ \mu$m width is created in less than 700 ps, most likely within the thermal runaway phase.

[1] R. L. Byer, Science **239**, 742-747 (1988).
[2] S. R. Ahmad and D. A. Russell, Propellants Explosives Pyrotechnics **33**, 396-402 (2008).
[3] S. A. Payne, C. Bibeau, R. J. Beach, A. Bayramian, J. C. Chanteloup, C. A. Ebbers, M. A. Emanuel, H. Nakana, C. D. Orth, J. E. Rothenberg, K. I. Schaffers, L. G. Seppala, J. A. Skidmore, S. B. Sutton, L. E. Zapata, and H. T. Powell, Journal of Fusion Energy **17**, 213-217 (1998).
[4] M. O. Ziegler, M. Münkel, T. Burkhard, G. Jennemann, I. Fischer, and W. Elsässer, J. Opt. Soc. Am. B **16**, 2015-2022 (1999).
[5] I. Fischer, O. Hess, W. Elsasser, and E. Gobel, Europhysics Letters **35**, 579-584 (1996).
[6] J. W. Tomm, M. Ziegler, M. Hempel, and T. Elsaesser, Laser & Photonics Reviews **5**, 422-441 (2011).
[7] M. Hempel, F. L. Mattina, J. W. Tomm, U. Zeimer, R. Broennimann, and T. Elsaesser, Semiconductor Science and Technology **26**, 075020 (2011).
[8] M. Hempel, J. W. Tomm, M. Ziegler, T. Elsaesser, N. Michel, and M. Krakowski, Applied Physics Letters **97**, 231101 (2010).
[9] M. Baeumler, J. L. Weyher, S. Muller, W. Jantz, R. Stibal, G. Herrmann, J. Luft, K. Sporrer, and W. Spath, in *Defect Recognition and Image Processing in Semiconductors DRIP VII 1997; Vol. 160*, edited by J. Donnecker and I. Rechenberg (Institute of Physics Conference Series, Templin, Germany, 1998), p. 467-470.
[10] H. Adachihara, O. Hess, E. Abraham, P. Ru, and J. V. Moloney, J. Opt. Soc. Am. B **10**, 658-665 (1993).
[11] D. E. Aspnes, S. M. Kelso, R. A. Logan, and R. Bhat, Journal of Applied Physics **60**, 754-767 (1986).
[12] J. Mukherjee and J. G. McInerney, Physical Review A **79**, 053813 (2009).
[13] M. Ziegler, M. Hempel, H. E. Larsen, J. W. Tomm, P. E. Andersen, S. Clausen, S. N. Elliott, and T. Elsaesser, Applied Physics Letters **97**, 021110 (2010).
[14] H. Fujii, Y. Ueno, and K. Endo, Applied Physics Letters **62**, 2114-2115 (1993).
[15] M. Hempel, M. Ziegler, J. W. Tomm, T. Elsaesser, N. Michel, and M. Krakowski, Applied Physics Letters **96**, 251105 (2010).